Supporting Information

pH Sensitivity of Interfacial Electron Transfer at a Supported Graphene Monolayer

Michel Wehrhold[*1], Tilmann J. Neubert[1,2], Anur Yadav[1], Martin Vondráček[3], Rodrigo M. Iost[1], Jan Honolka[3] and Kannan Balasubramanian[*1]

[1]School of Analytical Sciences Adlershof (SALSA), IRIS Adlershof & Department of Chemistry, Humboldt-Universität zu Berlin, Germany.

[2]Helmholtz-Zentrum Berlin für Materialien und Energie GmbH, Institut für Silizium-Photovoltaik, Kekuléstr. 5, 12489 Berlin, Germany.

[3]Institute of Physics, Academy of Sciences of the Czech Republic, Na Slovance 2, 182 21 Prague, Czech Republic.

* *Corresponding author e-mail* : Michel.Wehrhold@hu-berlin.de, nano.anchem@hu-berlin.de

Figure S1: Electrochemical etching (e-etching) of graphene. CVs of transferred graphene during e-etching, cycle 1 and 20 are compared here. The potential is scanned in a range of -0.6 to +0.2 V (vs. Ag/AgCl) in 100 mM HCl. The inset shows the oxidation of Cu^0 to Cu^{2+}, which is monitored to confirm the removal of copper. The red arrow at -0.6 V indicates the decrease in the oxygen reduction current, which occurs due to the removal of the copper traces. See Iost, et al. [1] for further details.

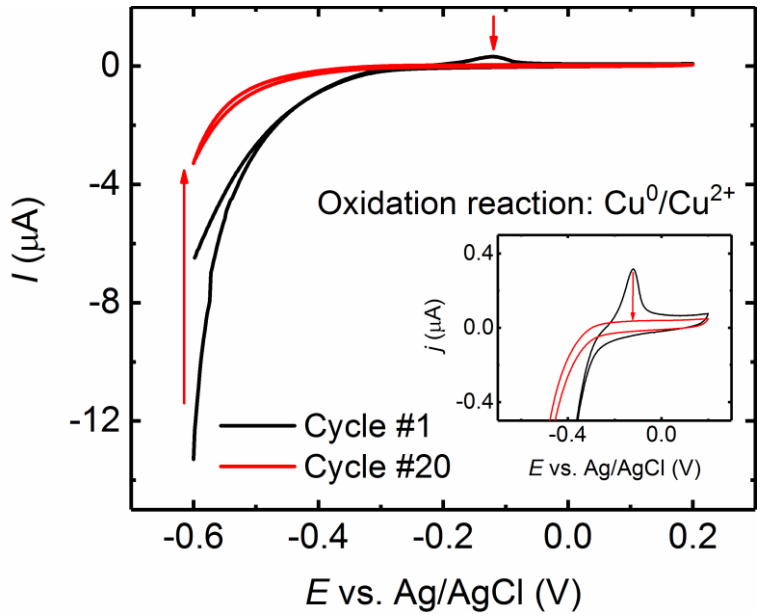

Fig. S2. Raman spectra of CVD-grown graphene monolayer on a range of substrate materials, normalized to the 2*D* peak intensity on the corresponding substrate. From bottom to top, the substrates are Si/SiO_2, Si/Si_3N_4, Al_2O_3 (*c*-plane sapphire) and gold (Au) surface. There is clear evidence of primary graphene peaks, *G* (1580 - 1587 cm^{-1}) and 2*D* (2630 - 2640 cm^{-1}) on all substrates. Additionally, the substrate peaks are also shown. The band between 930 and 1025 cm^{-1} on both Si/SiO_2 and Si/Si_3N_4 substrates is assigned to multiphonon scattering coming from the substrates. [2] The peaks 1374 and 1404 cm^{-1} on Al_2O_3 are also arising from the substrate itself. [3] In all cases, the *D*-peak (expected at 1320-1330 cm^{-1}) intensity is negligible. Laser excitation wavelength, λ_{exc} = 633 nm for aquisition on all substrates.

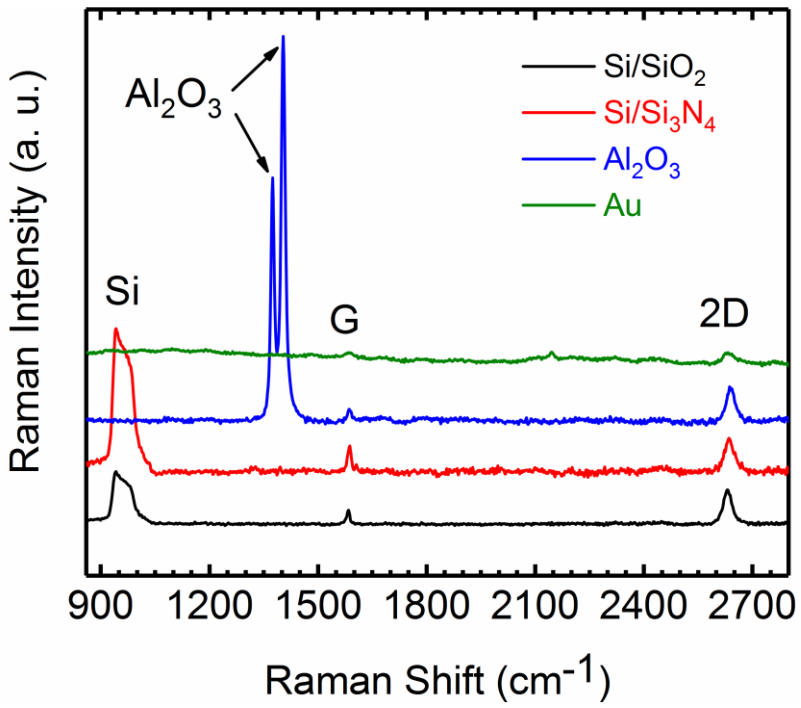

Fig. S3. The scan rate dependence of the redox probes before (black) and after (red) e-etching. The exploited redox probes are: a: 1 mM hexaammineruthenium, b: 100 µM ferrocence carboxylic acid, c: 1 mM hexachloroiridate, and d: 1 mM ferricyanide. All measurements were carried out in aqueous solutions containing 0.1 M KCl as supporting electrolyte.

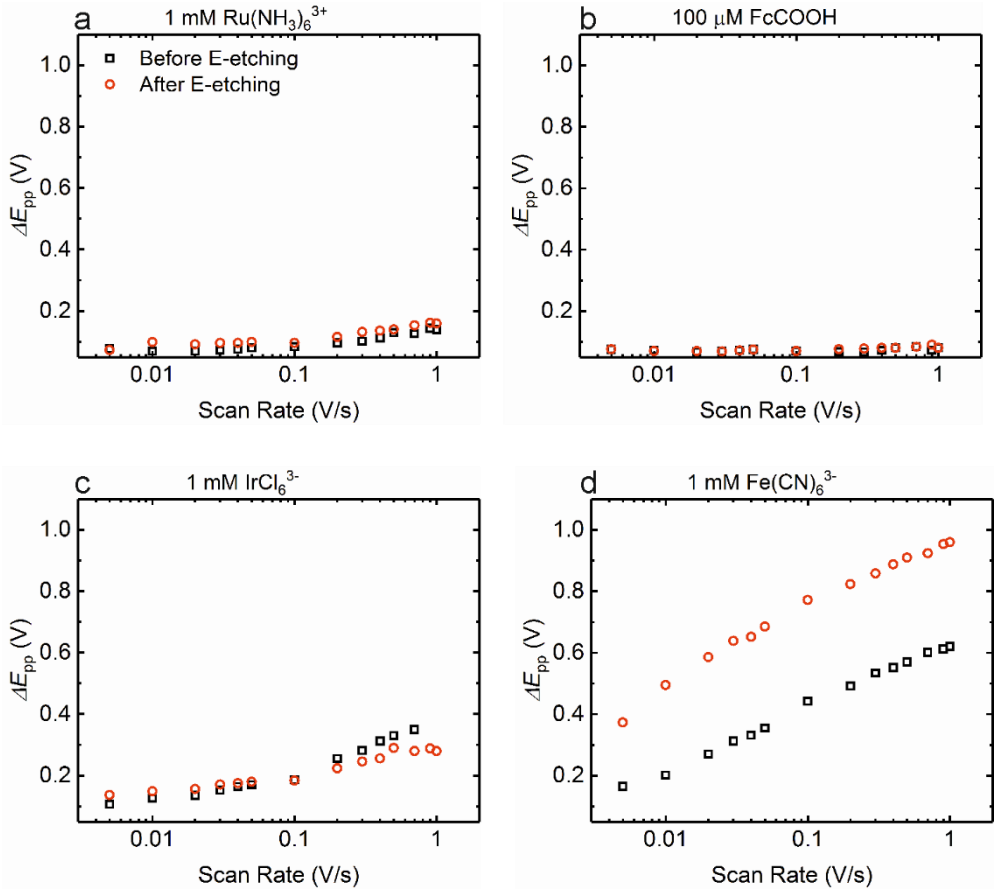

Table S1: Values of diffusion coefficients used for the estimation of the heterogeneous ET rate constant k^0 in table 1 in the main text using Nicholson [4] or Klingler & Kochi [5] methods.

Redox Probe	D_{Lit} **(cm^2/s)**	**References**
a $Ru(NH_3)_6^{2+/3+}$	$7 \cdot 10^{-6}$	6-11
b FcCOOH	$4 \cdot 10^{-6}$	12-13
c $IrCl_6^{2-/3-}$	$4 \cdot 10^{-6}$	10-11, 14
d $Fe(CN)_6^{3-/4-}$	$6 \cdot 10^{-6}$	6-7, 11, 15-16

Fig. S4. The formal potential (E_0') as a function of the pH value and in dependence of the supporting substrate of graphene and for metal electrodes. a: 1 mM hexachloroiridate, b: 1 mM ferricanide, c: 100 µM hexaammineruthenium, and d: 1 mM ferrocene carboxylic acid. All measurements were carried out in three different buffers with a different pH value. For this plot, a scan rate of ν = 100 mV/s was used.

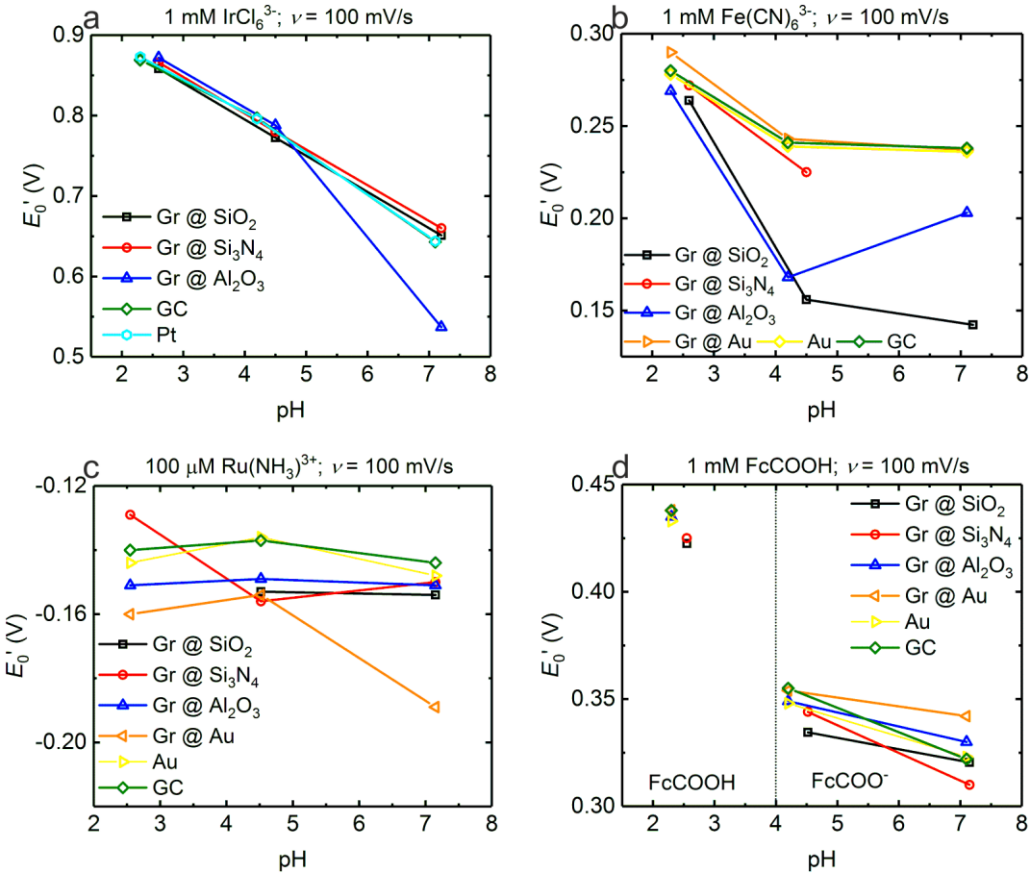

Fig. S5. The formal potential (E_0') as a function of the pH value and in dependence of the supporting substrate of graphene and for metal electrodes. a: 1 mM hexachloroiridate, b: 1 mM ferricanide, c: 100 µM hexaammineruthenium, and d: 1 mM ferrocene carboxylic acid. All measurements were carried out in three different buffers with a different pH value. For this plot, a scan rate of ν = 1 V/s was used.

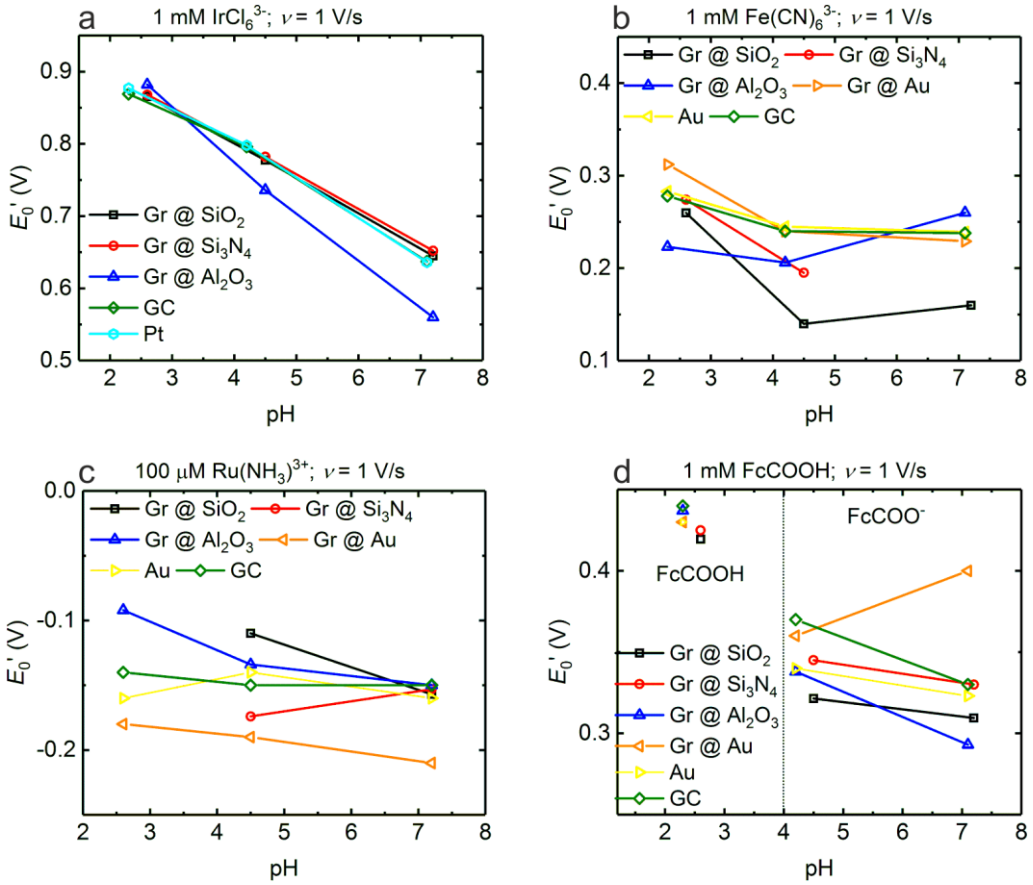

Fig. S6. Peak-to-peak separation (ΔE_{pp}) as a function of the pH value for graphene on various supporting substrates compared with metal electrodes. a: 1 mM hexachloroiridate, b: 1 mM ferricanide, c: 100 µM hexaammineruthenium, and d: 1 mM ferrocene carboxylic acid. All measurements were carried out in three different buffers with a different pH value. For this plot, a scan rate of ν = 100 mV/s was used.

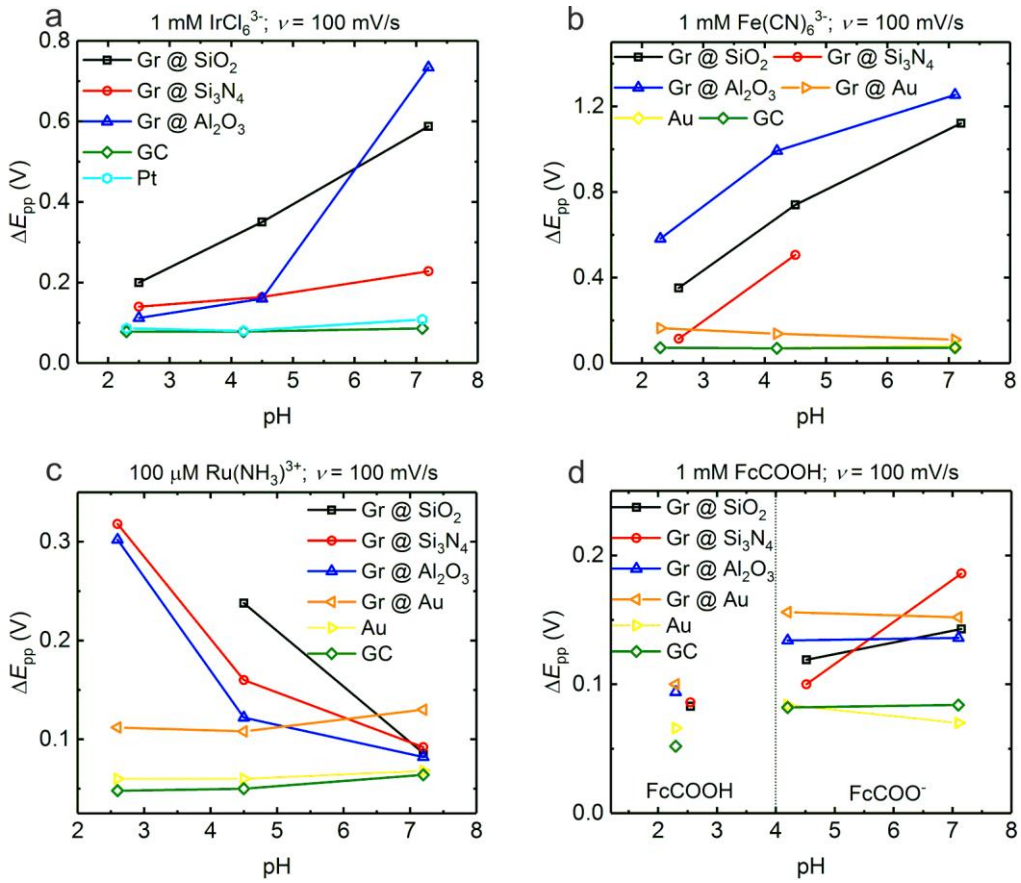

Fig. S7. Peak-to-peak separation (ΔE_{pp}) as a function of the pH value for graphene on various supporting substrates compared with metal electrodes. a: 1 mM hexachloroiridate, b: 1 mM ferricanide, c: 100 µM hexaammineruthenium, and d: 1 mM ferrocene carboxylic acid. All measurements were carried out in three different buffers with a different pH value. For this plot, a scan rate of ν = 1 V/s was used.

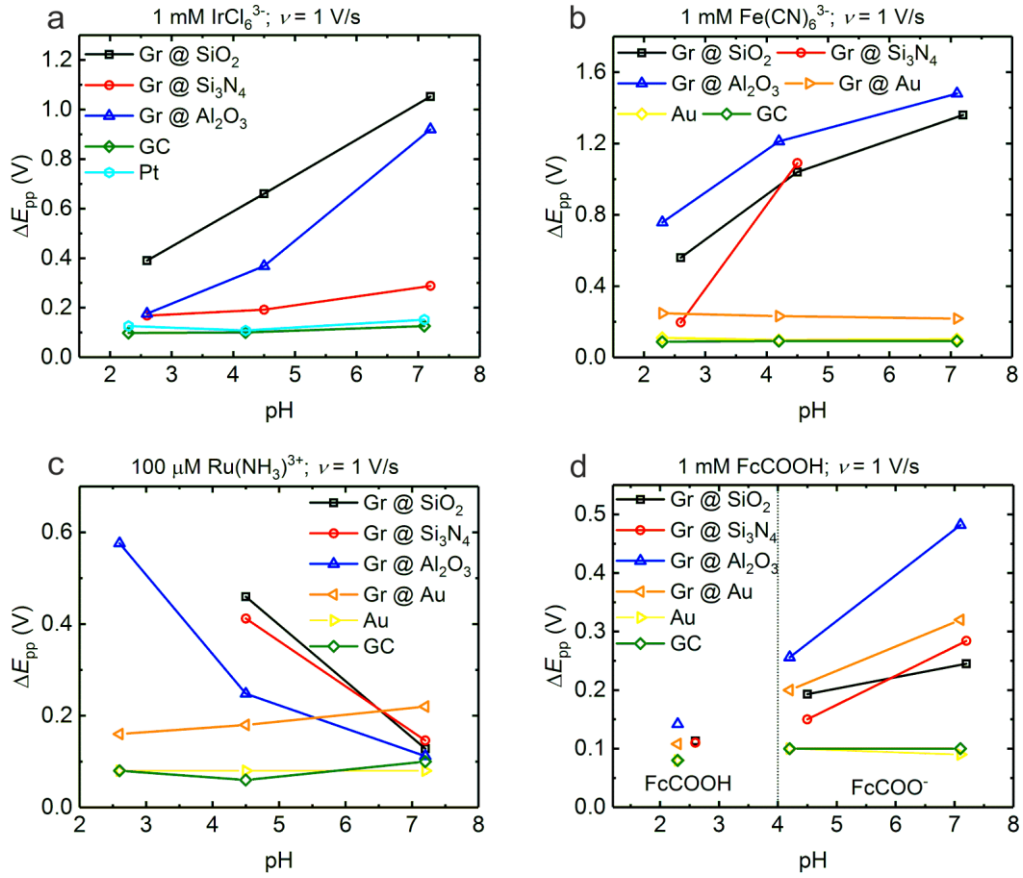

Fig. S8: Estimation of the surface charge distribution of graphene on Al_2O_3 using FET measurements. a: Dirac point as a function of pH. b: Estimation of the net surface charge at the GLI as a function of pH obtained by subtraction of V_{Dirac} at 250 mM (black line in a) from V_{Dirac} at 25 mM (red line in a).

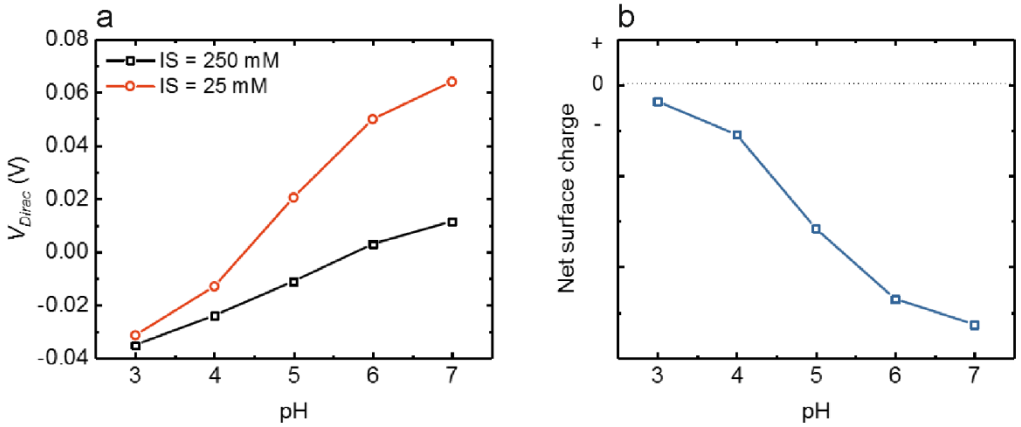

Figure S9: Electrochemistry of $Fe(CN)_6^{3-/4-}$ at a graphene monolayer transferred with hBN as supporting layer. a: pH-dependent CVs of graphene with hBN on top of Si/SiO_2 substrate. b: ΔE_{pp} as a function of the scan rate in different pH.

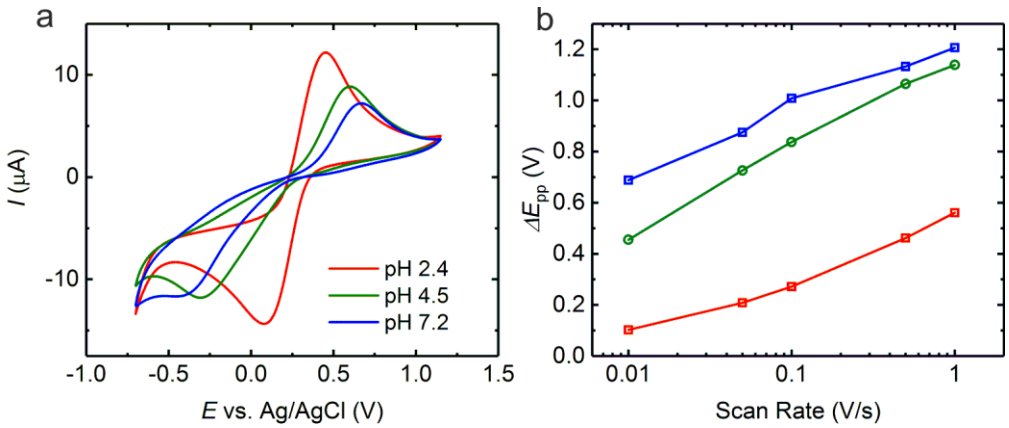

Fig. S10. Electrochemical measurements of Au supported graphene in comparison to a Au electrode. The measurements were carried out in three different buffers with different pH values. a: CVs of 1 mM ferricyanide, b: scan rate dependence of ΔE_{pp}, c: scan rate dependence of E_0'. d: CVs of 100 µM hexaammineruthenium, e: scan rate dependence of ΔE_{pp}, c: scan rate dependence of E_0'. g: CVs of 1 mM ferrocene carboxylic acid, h: scan rate dependence of ΔE_{pp}, i: scan rate dependence of E_0'.

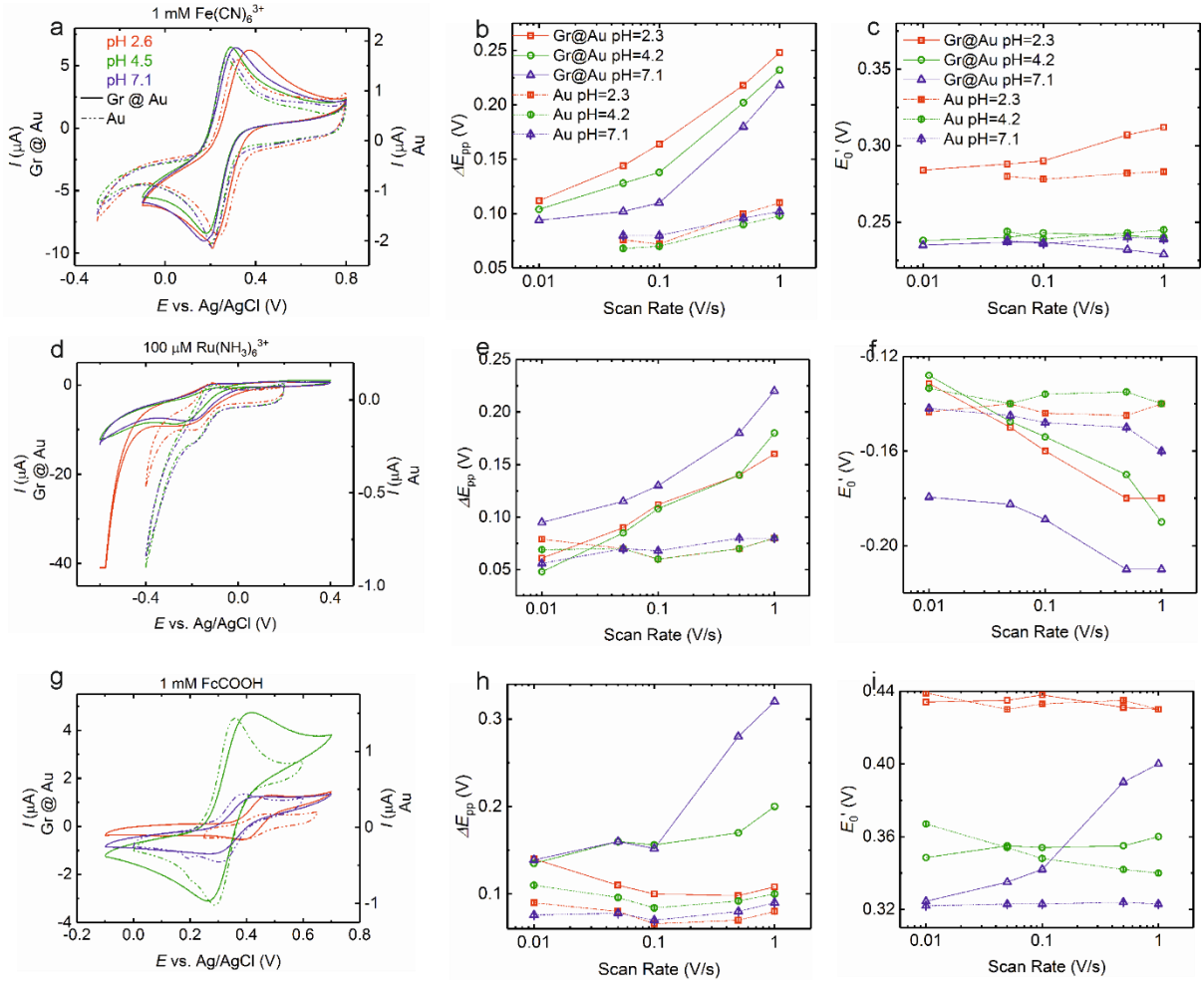

Table S2: The estimated apparent diffusion coefficients D_{app} for the four redox probes in different buffer solutions. The electrochemical measurements were performed using a circular GC electrode with a diameter of d = 1 mm. The evaluation of D_{app} was done exploiting the Randles-Sevcik relation.

Redox probe	D_{app} **(·10^{-6} cm^2/s)**		
	pH=2.5	**pH=4.3**	**pH=7.1**
$Fe(CN)_6^{3-}$	6.9	6.3	4.5
$IrCl_6^{3-}$	2.7	3.2	2.6
$Ru(NH_3)_6^{3+}$	37	32	32
FcCOOH	0.06	0.14	0.56

Figure S11. Comparison of XPS spectra measured on graphene on Si/SiO_2 and on graphene on Pt on the same sample, showing a systematic shift of around 1 eV due to the charging of the graphene flake on Si/SiO_2.

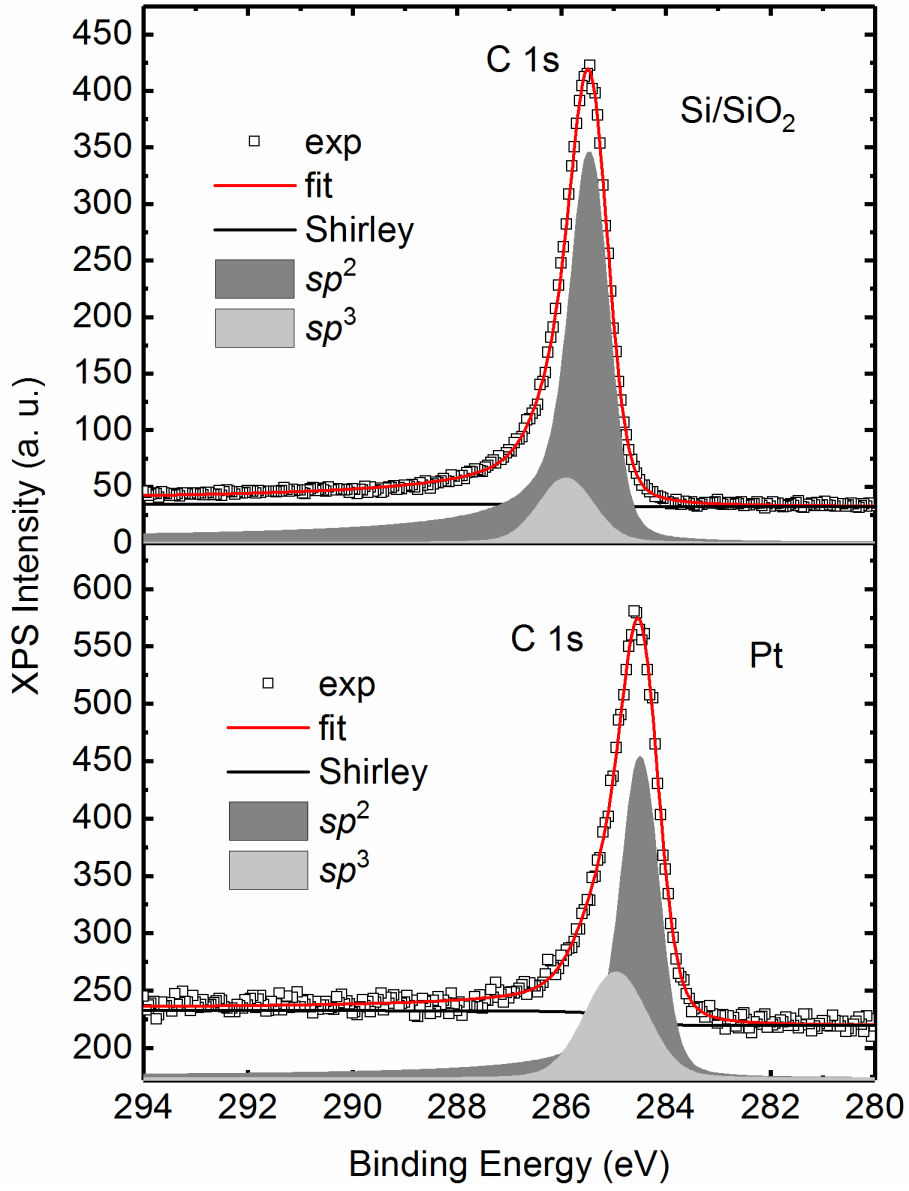

Figure S12. Alternative fitting of the high resolution C 1*s* XPS spectrum of figure 8 with an additional forced Voigt component shifted by +1.5 eV with respect to the sp^2 component. C1 and C2 corresponds to sp^2 and sp^3 components respectively, while C3, whose area amounts to around 4%, may be attributed to oxygen containing groups (C-O) in epoxy or hydroxyl units. Contributions from C=O can be excluded (within the detection limit) from the experimental data since there is no intensity at higher BEs (> 1.5 eV from the sp^2 peak). It could be argued that the C3 component is probably due to species such as C-OH. If this were true, we should see a much stronger pH dependence of the ET rates (by several orders of magnitude), due to the deprotonation of the hydroxyl group. Hence, we believe that the estimated actual density of 0.5% (see main text) of such ionizable species (participating in the interactions with the redox species) is much lower than 4% in our graphene samples. Another possible explanation is that the samples were brought to vacuum after long air exposure, and so the 4% may be due to ambient oxygen and carbon containing contaminants physisorbed on the sample before the XPS measurements, but possibly not present during the electrochemical measurements.

Taken together, the origin of the pH dependence of electron transfer may be due to trace amounts of ionizable groups, whose density is below the detection limit of XPS.

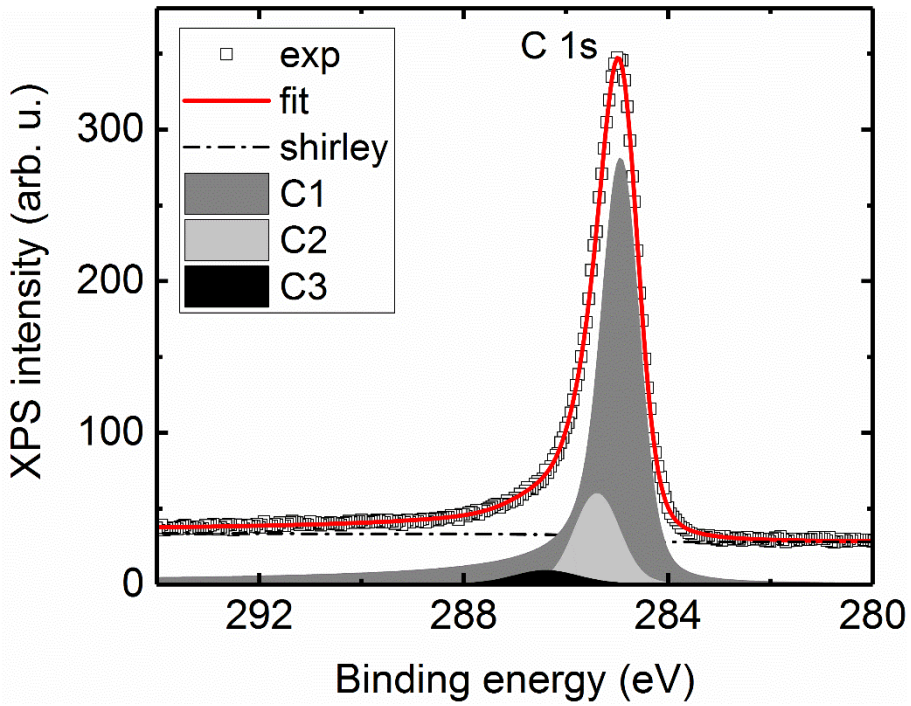

Figure S13: Simulation of the CVs using the conditions of figure 4 and the extracted rate constants (table 2) corresponding to $Fe(CN)_6^{3-/4-}$. The following parameters were used: E_0' = 0.268 V, α = 0.45, D_{app} = $6.9 \cdot 10^{-6}$ cm^2/s (red), D_{app} = $6.3 \cdot 10^{-6}$ cm^2/s (green), D_{app} = $4.5 \cdot 10^{-6}$ cm^2/s (blue), c_{Ox} = 1 mM and k^0 as indicated in the legend. Adsorption, double layer and electrostatic effects were not included. The simulation was done using *R* and is based on Brown. [17]

It is apparent here that with decreasing k^0 values (corresponding to decreasing ET rates in solutions of increasing pH), an increase in ΔE_{pp} , broadening of the waveshapes and reduction in the peak currents are observable, consistent with the trends observed in the experimental data. However, the magnitude of changes observed in the experimental CVs is higher. We conclude that this difference between the simulated and the experimental data comes from neglecting the electrostatic interactions and double layer effects in the simulation of the CVs.

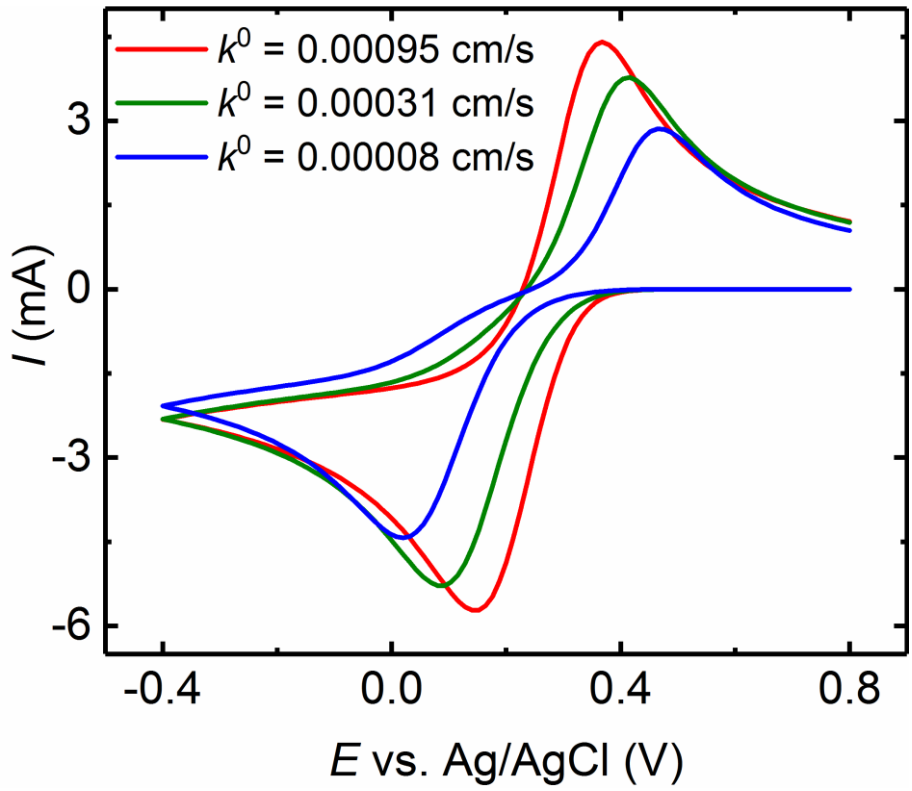

References

1. Iost, R. M.; Crespilho, F. N.; Zuccaro, L.; Yu, H. K.; Wodtke, A. M.; Kern, K.; Balasubramanian, K., Enhancing the Electrochemical and Electronic Performance of CVD-Grown Graphene by Minimizing Trace Metal Impurities. *ChemElectroChem* **2014,** *1* (12), 2070-2074.
2. Temple, P. A.; Hathaway, C. E., Multiphonon Raman Spectrum of Silicon. *Phys. Rev. B* **1973,** *7* (8), 3685-3697.
3. Wang, Q. H.; Jin, Z.; Kim, K. K.; Hilmer, A. J.; Paulus, G. L. C.; Shih, C.-J.; Ham, M.-H.; Sanchez-Yamagishi, J. D.; Watanabe, K.; Taniguchi, T.; Kong, J.; Jarillo-Herrero, P.; Strano, M. S., Understanding and controlling the substrate effect on graphene electron-transfer chemistry via reactivity imprint lithography. *Nature Chem.* **2012,** *4*, 724-732.
4. Nicholson, R. S., Theory and Application of Cyclic Voltammetry for Measurement of Electrode Reaction Kinetics. *Anal. Chem.* **1965,** *37* (11), 1351-1355.
5. Klingler, R. J.; Kochi, J. K., Electron-transfer kinetics from cyclic voltammetry. Quantitative description of electrochemical reversibility. *J. Phys. Chem.* **1981,** *85* (12), 1731-1741.
6. Plana, D.; Jones, F. G. E.; Dryfe, R. A. W., The voltammetric response of bipolar cells: Reversible electron transfer. *J. Electroanal. Chem.* **2010,** *646* (1), 107-113.
7. Banks, C. E.; Compton, R. G.; Fisher, A. C.; Henley, I. E., The transport limited currents at insonated electrodes. *PCCP* **2004,** *6* (12), 3147-3152.
8. Banks, C. E.; Rees, N. V.; Compton, R. G., Sonoelectrochemistry in acoustically emulsified media. *J. Electroanal. Chem.* **2002,** *535* (1), 41-47.
9. Marken, F.; Eklund, J. C.; Compton, R. G., Voltammetry in the presence of ultrasound: Can ultrasound modify heterogeneous electron transfer kinetics? *J. Electroanal. Chem.* **1995,** *395* (1), 335-339.
10. Velicky, M.; Bradley, D. F.; Cooper, A. J.; Hill, E. W.; Kinloch, I. A.; Mishchenko, A.; Novoselov, K. S.; Patten, H. V.; Toth, P. S.; Valota, A. T.; Worrall, S. D.; Dryfe, R. A. W., Electron Transfer Kinetics on Mono- and Multilayer Graphene. *ACS Nano* **2014,** *8* (10), 10089-10100.
11. Fischer, A. E.; Show, Y.; Swain, G. M., Electrochemical Performance of Diamond Thin-Film Electrodes from Different Commercial Sources. *Anal. Chem.* **2004,** *76* (9), 2553-2560.
12. Bartlett, P. N.; Pratt, K. F. E., A study of the kinetics of the reaction between ferrocene monocarboxylic acid and glucose oxidase using the rotating-disc electrode. *J. Electroanal. Chem.* **1995,** *397* (1), 53-60.
13. Cass, A. E. G.; Davis, G.; Francis, G. D.; Hill, H. A. O.; Aston, W. J.; Higgins, I. J.; Plotkin, E. V.; Scott, L. D. L.; Turner, A. P. F., Ferrocene-mediated enzyme electrode for amperometric determination of glucose. *Anal. Chem.* **1984,** *56* (4), 667-671.
14. Valota, A. T.; Toth, P. S.; Kim, Y.-J.; Hong, B. H.; Kinloch, I. A.; Novoselov, K. S.; Hill, E. W.; Dryfe, R. A. W., Electrochemical investigation of chemical vapour deposition monolayer and bilayer graphene on the microscale. *Electrochim. Acta* **2013,** *110*, 9-15.
15. Angell, D. H.; Dickinson, T., The kinetics of the ferrous/ferric and ferro/ferricyanide reactions at platinum and gold electrodes: Part I. Kinetics at bare-metal surfaces. *J. Electroanal. Chem.* **1972,** *35* (1), 55-72.
16. Winkler, K., The kinetics of electron transfer in Fe(CN)64−3− redox system on platinum standard-size and ultramicroelectrodes. *J. Electroanal. Chem.* **1995,** *388* (1), 151-159.
17. Brown, J. H., Development and Use of a Cyclic Voltammetry Simulator To Introduce Undergraduate Students to Electrochemical Simulations. *J. Chem. Educ.* **2015,** *92* (9), 1490-1496.